Nano-Structured Substrates for Single Cell Proteomics

Master Thesis in Nanosciences

Frank A. Zoller
frank.zoller@stud.unibas.ch

Laboratory for Micro- and Nanotechnology, Paul Scherrer Institut *and*
Maurice E. Müller-Institute for Structural Biology, Biozentrum, University of Basel

June 3, 2007

Supervisor: Prof. Dr. Andreas Engel
Maurice E. Müller-Institute, Biozentrum
University of Basel

Research Mentor: Dr. Celestino Padeste
Laboratory for Micro- and Nanotechnology
Paul Scherrer Institut, 5232 Villigen PSI

Abstract

Proteins are the main components of the physiological pathways of cells of living organisms. Proteomics, the large-scale study of these proteins, is crucial for the comprehension and modeling of biological processes on the molecular level. Single cell examinations are often required to gain quantitative understanding of the metabolism and signaling. For high-throughput biological research, array technology has become a powerful tool.

This work describes the nano-fabrication of substrates for a future proteomics chip. Combined with a read-out system based on an array of scanning probes, such chips should enable the specific and highly parallel detection of proteins down to the levels contained in single cells. Perfectly ordered and virtually defect-free lattices of several 10^4 anchor sites for the fixation of single cognitive proteins were produced. The anchor sites were gold islands, sitting on the bottom of beakers milled into the silicon dioxide coating of a silicon wafer by reactive ion etching. The capture sites were of a dimension close to those of the cognate proteins. For that purpose, the resolution of arrays of extreme ultraviolet interference lithography patterned holes with a pitch of 141 nm was improved by the glancing angle deposition of chromium and silver. After the evaporation of the gold islands, their final constriction in size and a reshaping was achieved by thermal annealing. The surfaces of the substrates were successfully passivated against the unintentional binding of biological macromolecules.

The designed substrates are geared to anchor state of the art capture proteins that facilitate a single protein detection limit and enable, together with the large number of capture sites, a chip with a dynamic range better than 10^4. Several 100 different proteins could be detected in parallel due to the compatibility of the substrates with 64 × 64 cantilever scanning probes.

Contents

Chapter 1

Introduction

1.1 Access to the Proteome

The dynamic complexity of biological processes is a tremendous scientific challenge. That is the reason why these processes are less well understood than many physical and chemical ones. In spite of an enormous progress, there are still wide gaps existing in the understanding of the disease pathogenesis and the development of effective strategies for early diagnosis and treatment [1]. However, this situation is about to change: the sequencing of a number of genomes and large-scale explorations of proteomes and metabolomes inspires hope that we will in the near future be able to describe a living creature in the strict language of mathematics [2].

The proteome is more complicated than the genome. Proteins undergo numerous ways of post translational modifications like e.g. phosphorylation, glycosylation, acetylation, and ubiquitination. A single gene can encode multiple different proteins – they can be produced by alternative splicing of the mRNA transcript, by varying translation start or stop sites, or by frameshifting during which a different set of triplet codons in the mRNA is translated. Hence, a proteome is considered to be at least one order of magnitude more complex than the genome [3].

In addition, proteins react to altered conditions by changing their location within the cell, by being cleaved into pieces and by adjusting their stability, as well as by the adaptation to different binding partners. Furthermore, protein levels hardly ever reflect mRNA levels and even the presence of an open reading frame does not guarantee the existence of a protein [4]. The protein composition of a cell is not static. Therefore, it is crucial to obtain quantitative comparisons with respect to changes in the environment of a cell. Not least, the knowledge of time scales of studied processes is essential for the modeling [5].

A deeper understanding of the signaling and the metabolomics requires a quantitative assessment of the behavior of single cells. Even the behavior of certain distinct ensembles – like their robustness – cannot be understood without access to the individual cell. The current proteomics research is a consecutive two-step procedure that commonly involves protein separation (typically two-dimensional gel electrophoresis) and analysis (e.g. mass spectrometry). These methods are simultaneously evaluating the relative abundance of numerous proteins but show difficulties by analyzing low abundance and membrane associated proteins [6]. To the best knowledge of the author, no method sensitive enough to explore single cells by proteomics is available. Optical single particle tracking techniques [7] only reach single molecule resolution using additional labeling. Neither state of the art cantilever arrays [8, 9], nor microarrays combined with modern waveguide technology [10], nor conventional AFM read-out systems [11] can reach the single cell detection limit.

1.2 Single Cell Proteomics

Besides the limitations in sensitivity, (micro-)array technology has become a crucial tool for large-scale and high-throughput biology. It allows the fast, easy and parallel detection of thousands of addressable elements in one single experiment. In proteomics the ultimate task is to analyze the entire complement of proteins expressed by a cell with such a chip. The proteome represents the physiological state on the protein level and correlates with intracellular and extracellular parameters [12, 13].

Behind this thesis stands the proposal to use the imaging capabilities of an atomic force microscope (AFM) to reach the described task [14]. Accordingly the challenge of having a sufficient throughput shall thereafter be achieved by a high degree of parallelism. A successful further development of the scanning probe array technique [15–17] accomplishing the requirements of single cell proteomics was already presented [18]. The application of large silicon probe arrays in an electrically conducting buffer solution necessitates a piezoresistive sensing system, which is well protected with silicon nitride films.

1.2.1 Designed Ankyrin Repeat Proteins

The recognition of the target proteins in this project will be mediated with designed ankyrin repeat proteins (DARPins) [19]. DARPins are engineered high-affinity binders with a broad range of potential applications, consisting of a few modules of a 33 amino acids consensus ankyrin repeat motif that are shielded with caps from

the γ-aminobutyric acid receptor β [20]. The repeat motif is held together by a self-assembling hydrophobic core and provides large, highly flexible binding surfaces. The consensus design was optimized for thermodynamic stability [21] and is very well expressed in soluble form in *E. coli* [19]. Combinatorial libraries of DARPins consisting of different numbers of the repeat motifs have been constructed [22]. DARPins have become a strong alternative to the widely used monoclonal antibodies [23], not least because they work without disulfide bridges. Furthermore, the binding affinities of the DARPins can be evolved towards more improved binding characteristics [24]. DARPins can be equipped with single cystein tags for the binding of gold, without influence on the expression yield. In addition, bispecific molecules, as well as fusions of DARPins with fluorescent proteins or other reporter proteins have been constructed.

1.2.2 Dynamic Range

Many essential proteins being part of signaling cascades can only appear in a number of a few dozens per cell. Others, e.g. the proteins of the cytoskeleton, relevant for the shape of the cell, show an occurrence which is several orders of magnitude higher. Unfortunately, there is no equivalent of the polymerase chain reaction that would enable the amplification of low abundance proteins. A valuable approach towards a single cell proteomics system has therefore to exhibit almost single molecule detection sensitivity and at the same time, offer a generic applicability to operate within a high dynamic range of several thousand fold.

1.2.3 Substrates

In this work, a potential mass fabrication procedure for substrates for single cell proteomics was explored. These substrates are designed to support the scanning probe read-out system and are compatible with DARPin-technology. The distinction between cognitive molecules that captured a target protein and the free binders can be facilitated, when the cantilever tip in the second case does not detect any topological information, except for a flat surface. This can be achieved by the fixation of the DARPins on the bottom of nano-structured wells with dimensions comparable to the size of the capture proteins. Such a well has to provide a chemically active area at its bottom to anchor a single or only a few binder proteins. Binding several capture proteins per spot would cause the disadvantage that the single protein detection limit could not be reached, since the AFM tip would only be able to distinguish between the situation that either any of the DARPins per anchor site had bound an analyte molecule or no single molecule had bound at all.

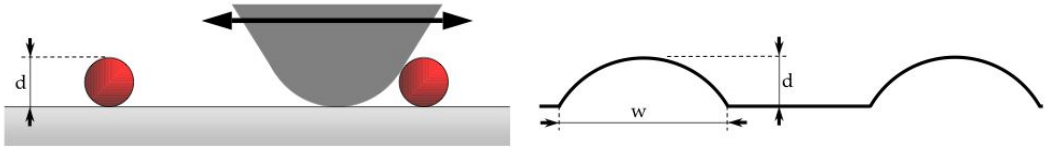

Figure 1.1: **Surface-Tip Convolution of a Scanning Probe Measurement.** The AFM scan does not reflect the topological information of the surface of an examined sample itself, but a convolution of the tip and the sample. The observed width w of a spherical object is given by $w = 2(2rd - d^2)^{1/2}$ [25], thereby is d the diameter of the object and r the radius of the scanning tip.

A major challenge of this proteomics project is to discriminate proteins bound by the cognitive molecules from the non-specifically bound ones. Besides the passivation of the substrates surface in between the capture proteins in order to diminish non-specific adherence, a key element of the design is the arrangement of the capture sites at precisely defined and well known positions. The nanostructured wells are located in a centered rectangular lattice, with a lattice constant of less than 200 nm, but big enough to enable the scanning probes to sense the substrate in between two different occupied capture sites (see also figure 1.1).

1.2.4 Anti-Adhesive Layer

Pursuant to our chip design, the surface area in between the capture proteins is three to four orders of magnitude larger than the surface covered with capture proteins. Brush-like films of poly (ethylene glycol) (PEG) form a barrier against the adsorption of macromolecules with outstanding qualities [26] as long as the grafting density is high enough [27]. Compression curves measured in a PEG brush-wall configuration show a strong repulsion upon compression and little adhesive force [28,29]. In addition, the films are highly lubricious. Both measures facilitate the usage as substrates for AFM.

PEG is, due to its water-solubility, a unique polyether [30]. PEG chains grafted to the surface at a sufficiently high density form a brush-like layer because the lateral interactions between the hydrated chains cause them to extend. The water content inside these surface-grafted layers is usually over 80 vol. % [31]. The grafting process restricts the density of the PEG brushes by repulsing the hydrated PEG chains. Therefore, the density of this films depend on the architecture of the polymers [32].

1.2.5 Potential Capacity of an Operating Chip

Current spotting technology is able to deposit material on fields of 100 × 100 µm. Such a spot of DARPins creates several 10^4 binding sites that can be operated with one cantilever of the probe array. An array of 64 × 64 cantilevers has the potential to monitor the expression of more than 1000 genes simultaneously, assuming a topological sensitivity of all scanning probes of the read-out system better than the dimensions of the analyte proteins. After having run calibration measurements, the surplus of fields, i.e. the redundancy of the types of capture proteins, facilitates the quantification of the analyte proteins. Different binders for the same target could also be used for the detection of protein complexes.

Dimensioning anchor points with a pitch of about 150 nm would allow the cantilever tips to reliably differentiate between two different binding sites and lead to a total number of 125.000 capture sites per field. The dynamic range of such a system promises to be higher than 10^4, since the presence or absence of a bound protein would be detected by the scanning tips with a certainty close to one. One cantilever had to scan 2500 μm^2, all anchor points for a distinct capture protein. A spacing of the width of the fields in between two fields would lead to a 40 mm^2 chip in the case of a 64 × 64 cantilever system. Homogenously mixing the content of one single cell, approximately 500 fl fluids and 10^9 proteins, is definitively demanding.

1.3 Nanostructuring Substrates

The ultimate resolution of optical lithography is always diffraction limited. Electron beam lithography (EBL) as well as focused ion beam lithography work with massy particles, compared to photons. The ions and electrons therefore have a surpassing low wavelength, that is in practice never resolution limiting. The handicap of focused ion beam lithography and EBL is – due to the serial nature of the methods – speed. On the other hand, these techniques allow feature sizes in the 10 nm range [33].

1.3.1 Alternative Nanopatterning Methods

Compared to EBL, two to tree times better resolution at the expenses of the application of an even much slower method can be realized, when an AFM tip is used to write the pattern, e.g. dip-pen nanolithography [34], nanopen reader and writer [35], nanoshaving [36], or nanografting [37].

A large area nanopatterning of functional binder proteins and a read-out system using height information was demonstrated [38] using colloidal lithography

[39,40]. For our purpose the ordering of the binding sites achievable with this technique would not be sufficient. The related nanosphere lithography [41] has the disadvantage that 10 nm feature sizes are hardly realizable. A dot arrangement in a equilateral triangular (hexagonal) lattice is only reachable using double-layered masks [42,43], which dramatically increases the difficulties of the formation of large and defect free particle arrangements. The evaporation of metal through a single layer of hexagonally close packed particles leads to a honeycomb lattice. The areas of perfectly ordered nanospheres are often small and contorted relative to the neighboring areas of highest ordering, which would make the read-out by AFM impracticable.

A direct printing of macromolecules using elastomeric stamps [44] is a popular technique for the creation of protein patterns. There exists a broad range of applications for microcontact printing, and also the nanometer range was exploited [45]. For our objectives the obtained dimensions and the compatibility with the post processing steps are, however not sufficient.

1.3.2 Extreme Ultraviolet Interference Lithography

Extreme ultraviolet interference lithography (EUV-IL, X-ray interference lithography) is a parallel technique offering the ability to outplay the structure sizes achieved with conventional ultraviolet optical lithography (see also figure 1.2) [46]. Interference lithography demands coherent light. Synchrotron sources deliver a sufficient coherence and a high brilliance at a broad range of the electromagnetic spectra. Two dimensional arrays of dots in photoresists can be produced by the interference of four beams, diffracted at linear transmission gratings [47,48]. Such a setup permits the formation of useful large two dimensional sinusoidal intensity distributions in the plane of the photoresist films and does so without transparent optical lenses. Duty cycles (ratio of feature size and pitch) better than one to two and pitches twice the frequency of the gratings are achievable. This leads to a very high resolution, when working with soft X-rays (extreme ultraviolet light, EUV).

1.3.3 Photoresist

Poly (methyl methacrylate)[1] (PMMA) has in this work been chosen as photoresist, because it is well established in nanofabrication and shows a good compatibility with the post processing steps, e.g. etch processes, oblique metal evaporation. Two other photoresists have been taken into account. Highly ordered self-assembled monolayers of 1,1'-biphenyl, either attached to silicon (4-hydroxy-1,1'-

[1] poly (methyl 2-methylpropenoate)

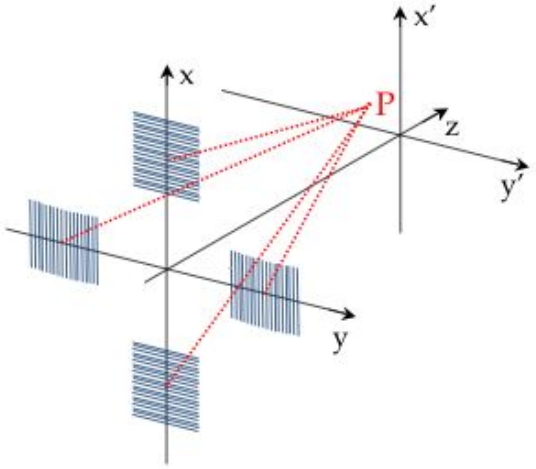

Figure 1.2: **Optical Path of Interference Lithography.** The four-beam interference lithography requires four diffraction gratings on a membrane in a plane (xy) orthogonal to the incident spatially coherent light (z). The diffracted beams overlap and form a sinusoidal interference pattern in the $x'y'$-plane. ($P \in x'y'$)

biphenyl, [49]) or to gold (4'-nitro-1,1'-biphenyl-4-thiol, [50]) substrates were shown to be good negative photoresists for chemical lithography. The resist offers a very good contrast between exposed und non exposed areas. The molecules crosslink under radiation and the nitro-terminated matrix converts into areas with terminal amino groups. This chemical contrast can be used for selective grafting of polymer brushes or immobilization of biomolecules [51–53]. In our case, a selective passivation of e.g. the exposed parts via a PEG-succinimidyl ester, would have been an interesting option. The big disadvantage of the presently existing biphenyl photoresists is their insensitivity against irradiation, close to the impracticable.

As a second alternative, hydrogen silsesquioxane [54,55], has been evaluated. Hydrogen silsesquioxane is a negative photoresist and therefore better suited for the production of pillars than holes. The radiation doses required to crosslink the molecules via SiH bond scission and silicon dioxide formation are higher than the ones needed to break the PMMA backbone. High aspect ratios can be obtained by the use of bilayer resists [56].

A big advantage of optical lithography compared to EBL is the small proximity effect. EUV photons do indeed create secondary electrons, but their mean path is in the range of merely 1 nm. Therefore the granularity of the photoresist – approximately 2.5 nm in the case of the widely used PMMA – becomes important as the limiting factor of the resolution. Due to our low demands regarding the complexity of the feature geometry and the trade-off between writing speed and resolution, EUV-IL, using PMMA as resist, was our choice.

Chapter 2

Materials and Methods

2.1 General

2.1.1 Chemistry

Unless stated otherwise, all chemicals were from Sigma-Aldrich (Buchs, SG, Switzerland). All open liquid and protein handlings were performed in a laminar flow box. The water was purified to a resistivity of 18.2 MΩ (Milli-Q Biocel, Millipore, Billerica, MA, USA).

2.1.2 Images

If not stated otherwise, the AFM scans were recorded in air with a Dimension 3100 (Nanoscope III, Veeco, Woodbury, NY, USA) in tapping mode, using silicon cantilevers (NSC15/Al BS, MikroMasch, Tallinn, Estonia). A NanoWizard (JPK Instruments, Berlin, Germany) and OMCL-TR 400 cantilevers (Olympus, Tokyo, Japan; stiffness: 0.08 N/m) were used to image in liquid. With both instruments, 1024 data points per scan line were recorded at line frequencies of 0.8 – 2 Hz.

The scanning electron microscopy (SEM) images were recorded with a Zeiss Supra 55 VP (Zeiss, Oberkochen, Germany), using in-lens detectors, a working distance of 3 – 4 mm, 5 – 7 kV acceleration voltage, and a 30 µm aperture.

Fluorescence pictures were taken with an Axiophot (Zeiss, Oberkochen, Germany) stereo microscope with top illumination, a 488 nm optical filter and a Kappa Camera (Opto Electronics, Gleichen, Germany). The samples covered with fluorescent dyes were blow dried before analyzing them.

2.2 Patterning

2.2.1 Lithography

The production of the substrates was started by spin coating (4000 – 6000 rpm, 45 s) PMMA resist (650 kDa, 1.3 % in chlorobenzene) onto a single side polished 4 inch silicon wafers with a 120 nm thick thermal oxide layer. Then, the wafer was baked on a hot plate (160 C, 180 s), before transferring it into the vacuum chamber of the X-ray Interference Lithography beamline [48] of the Swiss Light Source (PSI, Villigen, Switzerland). EUV exposures were done in vacuum ($< 10^{-5}$ mbar) using highly special coherent undulator light with a central wavelength of 13.1 nm (92 eV) and 3 % spectral bandwidth. The incident EUV power on the substrate was several mW/cm^2 and the delivered dose was controlled in the range of 120 – 420 mJ/cm^2 using a fast beam shutter. Typically areas of 400 × 400 µm were patterned in a single exposure by multiple beam diffraction. The masks used to produce the interference pattern were chromium gratings on free standing silicon nitride membranes, fabricated in-house using EBL.

Unless stated otherwise, all exposed patterns were fully automatically spray developed by a HamaTech (Steag, Sternenfels, Germany) in a 1:3 methyl isobutyl ketone[1] (MIBK):isopropyl alcohol[2] (IPA) solution for 30 s.

2.2.2 Wafer Processing

The wafer with the developed structures was diced into pieces or broken by the use of diamond scribers. Each piece contained a series of individual exposures covering the whole intensity range. The oxygen plasma treatment for cleaning and for the activation of the surfaces of the wafer pieces was performed in a Plasmalab 80 Plus (Oxford Instruments, Witney, Oxon, UK) at 100 mTorr O_2 pressure and with 150 W forward power. Cleaning in organic solvents included sonicatation of the substrate in a actetone bath and subsequently in an IPA bath. Thereafter the substrates were rinsed and blow dried.

2.2.3 Metal Evaporation

For the deposition of metals a Balzers BAE 250 (Oerlikon Balzers, Balzers, Lichtenstein) evaporation system was used. Prior to starting the evaporation process, the chamber pressure was decreased to less than $6{\cdot}10^{-6}$ mbar. The distance between the

[1] 2-methylpentan-4-one
[2] propan-2-ol

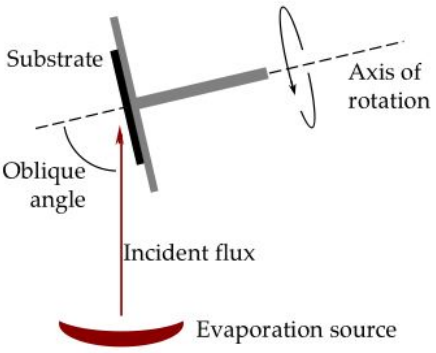

Figure 2.1: **Glancing Angle Deposition.** Experimental setup for the evaporation of the GLAD masks on top of the EUV-IL patterned PMMA.

source and the substrate was approximately 30 cm. All evaporated metals were from ChemPur (Karlsruhe, Deutschland) and had a purity better than 99.9 %.

In order to narrow the openings of the hole patterns in the PMMA, gained by lithography, glancing angle deposition (GLAD) [57,58] was used. The substrates were tilted to a highly oblique angel between 60° and 80° relatively to the incident flux and were concurrently, continuously rotated along a normal of the substrate with a rotational speed of approximately 120 rotations per minute. The figure 2.1 visualizes the experimental geometries. The deposition rate was set between 0.2 and 5 nm/s and was measured on a plain normal to the incident flux through the sample, by a quartz crystal microbalance.

Gold was deposited in an orthogonal orientation with respect to the flux of metal. The deposition rate was stabilized at 0.7 – 1.5 nm/s before a shutter was opened and the deposition process on the samples was started.

2.2.4 Etching & Lift-off

The EUV-IL patterns were transferred into the silicon oxide coating of the substrates by reactive ion etching (RIE) with a Plasmalab System 100 (Oxford Instruments, Witney, Oxon, UK), using SF_6 (8 – 40 sccm) or a combination of CHF_3 (40 sccm) and O_2 (3 sccm). Before starting the etch routine, the chamber of the instrument was preconditioned by running the later etch program on a dummy wafer. The etch gases were let into the chamber, after evacuating it to 5.5^{-5} mTorr. The plasma was performed at a pressure of 20 – 100 mTorr, using 25 – 100 W forward power. The substrates temperature was held in the range of 300 K ± 2 K. After switching off the plasma, the chamber was flushed with argon.

Chromium was wet etched in a solution of ceric ammonium nitrate (5 % in diluted acetic acid) at pH 6. If not stated otherwise, the lift-off was performed in a

series of three baths of fresh dichloromethane. The substrate was sonicated during the first two bathes. Then the sample was blow dried.

2.2.5 Annealing

The annealing of the evaporated gold islands [59] was either performed in the Balzers evaporation system (see chapter 2.2.3) in vacuum (10^{-5} – $2{\cdot}10^{-5}$ mbar) using an in-house designed insertion described elsewhere [60] or in a high-temperature furnace (Labortherm N3, Nabertherm, Lilienthal, Germany) at atmospheric pressure in air. In the vacuum chamber the substrates were heated from ambient temperature to 512 C within 40 minutes. The temperature was held at the maximum for 20 minutes, thereafter it was lowered to room temperature again within a period of 20 minutes. In air, the samples were heated up within 60 minutes. The temperature was then held at the peak for 10 minutes. Afterwards, the samples were cooled down to room temperature within 20 minutes.

2.3 Surface Modification

2.3.1 Non-Adhesive Layers

Two different commercial products were used to passivate the free silicon oxide surface areas against non specific binding of biomolecules: a star shaped PEG molecule [64–67] (Hydro-Stellan N612K, SusTech, Darmstadt, Germany) and poly (L)-lysine (PLL) grafted PEG [61–63] (PLL-PEG; SurfaceSolutions, Zürich, Switzerland).

As the test samples, silicon dioxide covered silicon wafer pieces were used. The wafer was regularly striped with 15 – 90 µm broad gold bands, produced by photolithography and etching. The interspace in between the bands was as broad as the bands themselves. The gold bands were 12 nm high and sat on top of 3 nm of chromium adhesion layer. As an unstructured alternative for the examination of adsorption, mica template-stripped large atomically flat gold samples [68] were used.

PLL-grafted-PEG A PLL-PEG with an average PLL backbone length of 96 monomer units, a grafting ratio of 3.5 lysine monomer units per grafted PEG chain and a molecular weight of 2 kDa per PEG chain – which promised to be the optimal architecture for protein-resistance [69] – was chosen. These polymers were dissolved in 10 mM HEPES[3], 150 mM NaCl buffer (pH 7.4) at a concentration of 0.5 mg/ml and

[3] 4-(2-hydroxyethyl)piperazine-1-ethanesulfonic acid

filtered trough a 0.22 µm poly (tetrafluoro ethylene) (PTFE) membrane. The polymer solution was divided into aliquots and stored at -20 C until use.

The substrates were cleaned by oxygen plasma before 100 µl per cm^2 thawed polymer solution was pipetted onto them. At pH 7.4 the silicon oxide surface exhibits negative charges. An oxygen plasma treatment intensified this effect. The chosen PLL-PEG concentration is about 5000 times higher than needed for the formation of a monomolecular adlayer, based on quantitative nuclear magnetic resonance data and optical waveguide lightmode spectroscopy [70]. For the period of 30 minutes, the substrates were stored on pillars fixed inside the bottoms of the beakers of six-well plates at room temperature. The beakers were partly filled with buffer solution and the wells covered to avoid the desiccation of the substrates. The PEGylation was finished by rinsing the substrates in water and blow drying them.

Star PEG A dose of 50 mg 1 kDa Hydro Stellan Star PEG was dissolved in 1 ml tetrahydro furan and poured into 9 ml stirred water. After 5 minutes, the solution was filled up in a single-use syringe and after a well defined time dribbled trough a 0.22 µm PTFE membrane filter onto the substrate sitting on a spinner. Then the substrates were accelerated with 500 rpm/s and spinned for 40 s.

2.3.2 Passivation of Gold

Mercaptoundecanoic acid (MUA), N-(2-mercaptopropionyl) glycine (MPG), and sodium 2-mercaptoethane sulfonate (MES) were used to deactivate gold surfaces. All three thiols were applied in 10 mM concentration, MES and MPG in water, MUA in ethanol. The substrates were incubated for 30 minutes by the thiol solution, sitting on pillars fixed in bathes of the corresponding solvent. After incubation, the samples were carefully rinsed. When combined with PEGylation, the thiols were applied at first.

2.3.3 Protein Adsorption

During the absorption of proteins, the substrates were put onto pillars fixed on the bottoms, inside the beakers, of covered six well plates. The beakers were partly filled with the same buffer solution, that the proteins were diluted in. 50 µl protein solution was pipetted onto the substrate per cm^2 surface area. 30 minutes after applying the protein, the sample was rinsed with buffer. The harsher cleaning step included an additional rinsing step with 0.5 % Tween20, before washing with buffer again. If not stated otherwise, the proteins were all stored at -20 C until use.

DARPins C-terminally GGGSGGGS-cysteine tagged off7 and mbp3_16 DARPins (300 and 280 µM, respectively in 50 mM Tris · HCl, 500 mM NaCl, 260 mM Imidazole, 10 % glycerole, pH 8.0) [22] were reduced with in an equivalent volume of Tris (2-carboxyethyl) phosphine bond-breaker solution (Pierce, Rockford, IL, USA) overnight. The DARPin solutions were then diluted in 50 mM Tris · HCl, 500 mM NaCl, pH 8.0 to a final concentration of 10 µM.

Maltose Binding Protein Before applying N-terminally biotinylated maltose binding protein (BMBP) onto the DARPin exposed samples, the solution (25 mM Tris · HCl, 250 mM NaCl, pH 8.0) was diluted within the same buffer to a final concentration of 20 µM.

Fluorescent Avidin Alexa Fluor 488 (Invitrogen, Carlsbad, CA, USA) labeled Avidin was used in a concentration of 10 mg/l in 50 mM PO_4^{3-}, pH 7.0, when directly applied to the surface, or in a 40 mg/l concentration, when suggested to bind BMBP. The labeled Avidin was stored in a 10-fold stock at 3 C.

Chapter 3

Results

Gold islands were chosen as anchor points for the capture proteins. The DARPins can be fixed via a cysteine tag. The golden capture sites showed to be fully compatible with all post precessing steps and inert to harsh cleaning protocols. Untreated features gained by state of the art EUV-IL were larger than the dimensions of a protein. Therefore this features had to be constricted in size by additional procedures.

3.1 Interference Lithography

3.1.1 Mask Design

The chamber and mask geometries at the X-ray Interference Lithography beamline were adjusted to produce first-order interference patterns with doubled frequency compared to the diffraction gratings. In this work, gratings with a 200 nm periodicity and a gratings-wafer working distance of 3 mm led to the best results. Thereby, the uniformity of the pattern over the whole array, as well as the slope of the walls of the produced holes were especially taken into consideration. When interfering four beams, sufficiently large 141 nm patterns could be produced. It was shown, that a simple aperture plate mounted parallel to the diffraction mask, behind the membrane supporting the gratings, was able to block effectively and selectively the non-diffracted or unprofitably (higher than first-order) diffracted light (see figure 3.1). Large areas of full PMMA exposure could be avoided this way and two arrays of interest (141 nm hole pattern) could be positioned closer to each other. A separation in the range of the diameter of the arrays was feasible. Alignment marks were successfully produced by the creation of windows in the aperture plate and in the chromium coating of the membrane, respectively.

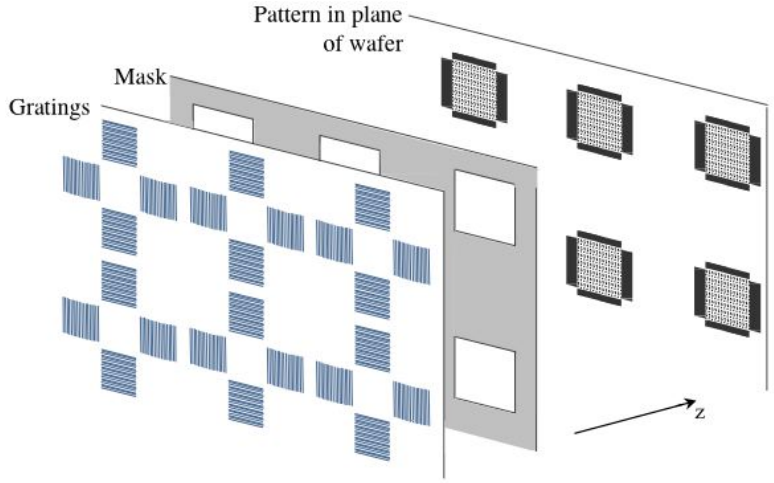

Figure 3.1: **Aperture Plate as Part of the EUV-IL Mask.** Only the use of an aperture plate (mask) that blocks highly diffracted and non diffracted light enables to arrange different hole patterns close to each other. In the illustrated setup, the hole pattern on the wafer are surrounded by rectangular areas of full exposure (non diffracted light, visualized in dark).

3.1.2 Photoresist

Because of the limitations of GLAD, a basic requirement to achieve 10 nm gold islands was the production of EUV-IL patterns with a duty cycle better than 1:3, with reference to a 141 nm pitch of the hole arrays. A crucial element was thereby the thickness of the EUV resist PMMA. EUV-IL exposed and developed samples did not have holes with vertical walls. The diameter of the opening on top of the PMMA layer was the starting point for the subsequent constriction by GLAD and defined the final dimensions of the islands. Thinner resist layers therefore led to smaller final structures. A too thin PMMA layer caused problems because the obliquely evaporated metals got into contact with the surface of the wafer and made a lift-off of deposited metal impossible. A resist thickness of 40 nm outperformed the results achieved with 70 nm PMMA coatings and was close to the limit of not causing lift-off difficulties.

3.1.3 Development

It was reported that cold development techniques could be used to decrease the size of the features of the smallest EBL patterns by a factor of two compared to the ambient [71,72]. The low temperature decreased the reactivity of the organic solvents of the developers. Higher clearance doses were required. The influence of the proximity effects was decreased. Cold development was reported to increase the contrast best by cooling the solvent (1:3 MIBK:IPA with 1.5 vol.% methyl ethyl ketone) to -6 C [72]. Our experiments showed that these improvements in connection

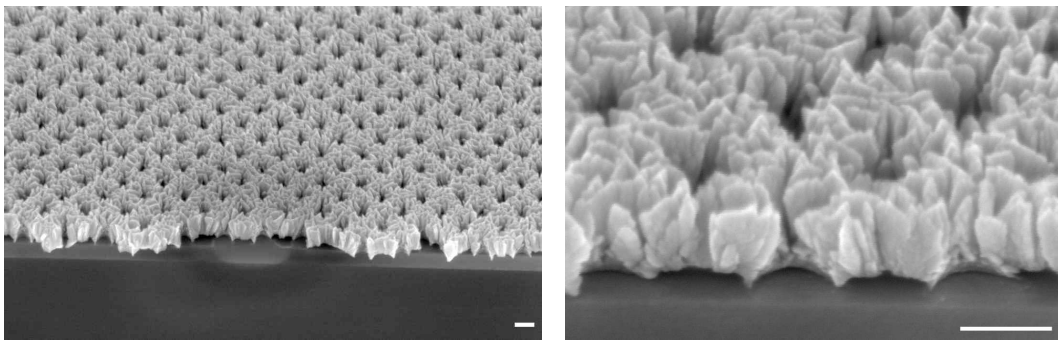

Figure 3.2: **Chromium GLAD Mask.** The SEM images show a cross section through a 100 nm thick GLAD chromium mask, evaporated at an oblique angle of 70° on a hole array (141 nm pitch) patterned by EUV-IL. (scale bars: 100 nm)

with EBL can not be transferred to EUV-IL. The line edge roughness of the EUV-IL was not significantly increased.

As another method to surpass the ultimate resolution of EBL, ultrasonically-assisted development in a 3:7 water:IPA mixture was proposed [73]. Water:IPA solutions are intrinsically poor developers and decrease the sensitivity. The swelling of the unexposed resist should be avoided. However, we could not find any improvements compared to the standard development when applying this protocol on EUV-IL patterned samples.

3.2 Glancing Angle Deposition

Due to the stochastic grain formation and self shadowing effects, the thickness of the GLAD mask (see figure 3.2), that had to be evaporated in order to close a hole of a distinct size in the PMMA completely could not be calculated by just using an elementary geometrical approach. The opening of a hole with a diameter of 85 nm could in average be constricted to 20 nm, by the deposition of a 100 nm thick metal layer, using an oblique angle of 65°. This was the maximal possible thickness, as any further evaporation caused the complete closure of the first holes of the array. The degree of constriction that could be performed by GLAD depended on the uniformity requirements of the narrowed holes. The important cross-section of the openings strongly depended on slight inequalities of the GLAD mask when it was constricted to only a few nm in diameter. If the observed variability of the cross-section had to be less than 10 %, a constriction of the EUV-IL patterned holes by more than a factor of three was not realizable.

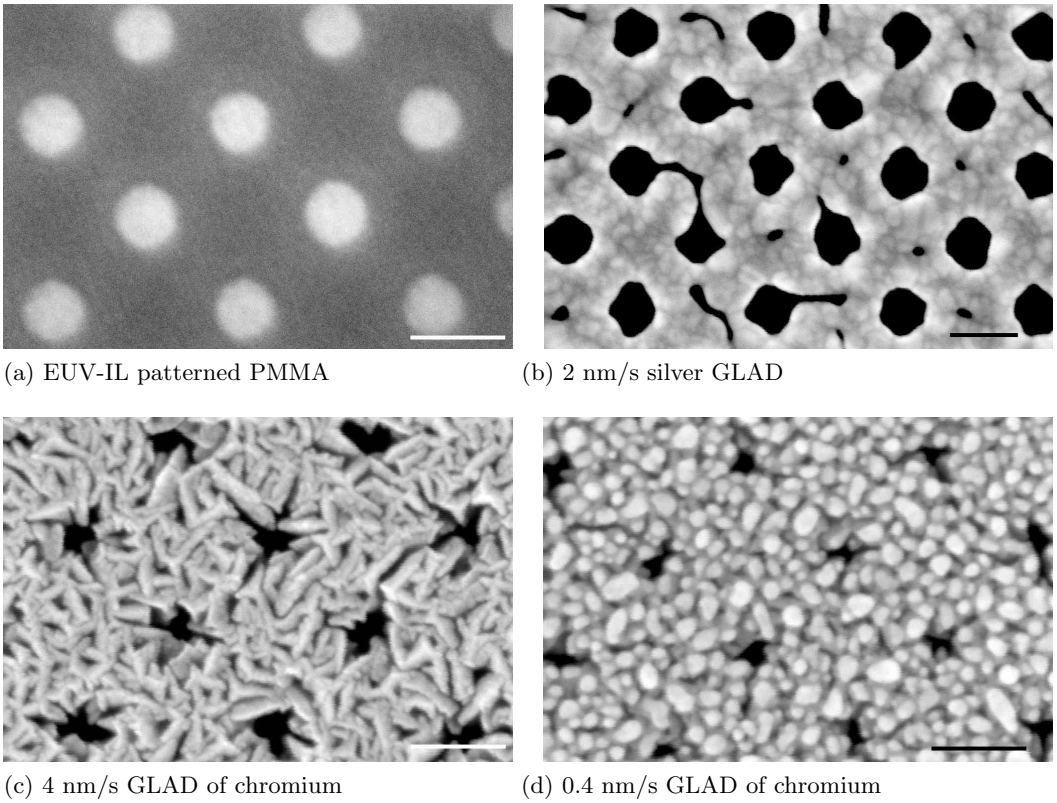

(a) EUV-IL patterned PMMA

(b) 2 nm/s silver GLAD

(c) 4 nm/s GLAD of chromium

(d) 0.4 nm/s GLAD of chromium

Figure 3.3: **Variations of GLAD Conditions.** The GLAD of silver leads to smooth masks that constrict the EUV-IL patterned holes in PMMA few, as the comparison of the images of the coated (figure 3.3b) and untreated (figure 3.3a) samples show. The images 3.3c and 3.3d illustrate the effect of the deposition rate of the GLAD of chromium on the graininess of the achieved masks. (scale bars: 100 nm)

3.2.1 Evaporated Metal

Metals with low boiling points can be thermally vaporized in our evaporation chamber. Silver[1], aluminum[2], chromium[3] are amongst the commonly used metals with the lowest boiling points. All three were tested as substances for GLAD. The promising element titanium[4] could not be used, because of its high boiling temperature. Chromium led to the best constriction of the holes. The formed layers were rather grainy. Silver and aluminum constricted less well and formed both similarly smooth layers (see also figure 3.3). This advantage was in both cases facilitated by the high fluidity of the deposited metal. The big drawback of this fluidity were lift-off problems caused by the contact of the metal and the surface of the wafer. Below a certain oblique angle, the lift-off became totally impracticable.

[1] 2162 C, standard conditions [74]
[2] 2519 C, ditto
[3] 2671 C, ditto
[4] 3287 C, ditto

3.2.2 Deposition Rate

Concerning the handling, silver outperformed aluminum because of the better controllability of the deposition rate. Aluminum tended to evaporate in an explosion like process. Most probably, an oxide layer on top of the melted metal inhibited its steady evaporation. When the temperature was increased high enough, the oxide broke and the underneath metal vaporized rapidly. Silver was best evaporated with a speed of 4 – 5 nm/s. The high rate insignificantly increased the granularity but compensated the negative effect of the fluidity of the metal. The figures 3.3c and 3.3d show the major impact of the deposition speed on the graininess of the chromium coatings. A high deposition rate of 5 nm/s led to a layer of needle like crystals. The shape of the clusters formed by a speed of only a few hundred pm/s appeared spheroidal and small.

A small size of the grains was desirable, since it resulted in a more distinct uniformity of the pattern. The disadvantage of a low deposition speed was the strong rise of the temperature of the photoresist on the substrate. PMMA can be deformed plastically above 100 C and melts when heated to temperatures higher than 135 C. The best compromise between the constitution of the mask and the protection of the photoresist was achieved at a value of 1 nm/s for chromium. The pressure in the evaporation chamber was another important parameter that had an impact on the graininess of the deposited layers. A too high pressure ($\gg 10^{-5}$ mbar) resulted in a rougher mask, due to an increased formation of clusters and the oxidation of the deposited surfaces.

Bi-metallic GLAD masks were produced successfully (see figure 3.4a). Firstly, chromium was evaporated, causing the major constriction of the opening. Secondly, silver was deposited to increase the smoothness and homogeneity of the mask.

3.2.3 Oblique Angle

The angle, at which the evaporated metal particles impinged on the substrate had an influence on the degree of constriction. Oblique angles in the range of 80° hardly closed the openings. On the other hand, angles smaller than 60° ± 3° in the case of chromium and 70° ± 4° in the case of silver caused severe lift-off problems, since the evaporated metal got into contact with the surface of the wafer. These minimally practicable angles depended on the precise geometry (ratio of coating thickness and hole size) of the EUV-IL patterned holes in the PMMA layer. When producing combined chromium-silver masks, the oblique angle, at which the second metal silver was evaporated, could be decreased by 5°. The

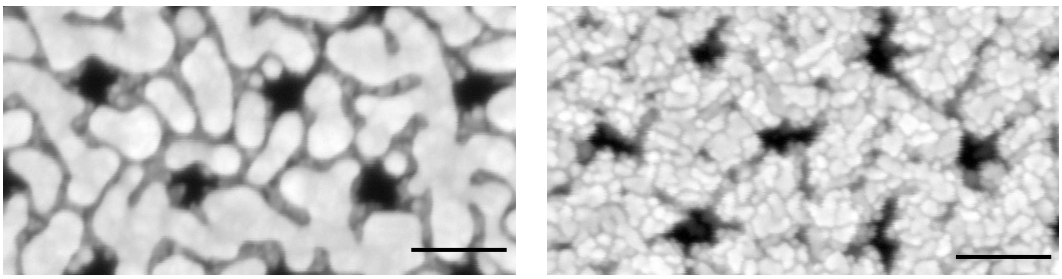

(a) bi-metallic chromium-silver GLAD
75 nm Cr (0.4 nm/s, 65°) & 30 nm Ag
(2 nm/s, 70°)

(b) chromium-silver-chromium multi-layer GLAD
60 nm Cr (0.3 nm/s, 75°) & 25 nm Ag
(4 nm/s, 75°) & 50 nm Cr (1 nm/s, 75°)

Figure 3.4: **Chromium-Silver Multi-Layer GLAD.** The evaporation of a silver layer by GLAD upon a chromium GLAD mask smoothened the coating and led to more uniform holes (see figure 3.4a). The precise dimensions and the varieties of the golden capture sites could not be determined by the imaging of the GLAD masks. The evaporation of gold and the lift-off of the masks was required. Problems with the chromium etch step of the lift-off process could not be avoided using chromium-silver-chromium multi-layer GLAD masks (see figure 3.4b). (scale bars: 100 nm)

first chromium layer had a modifying effect on the geometries that facilitated the prevention against an irreversible connection of the metallic mask and the silicon dioxide surface of the wafer.

3.3 Leveling of the Topology

The plunging of the later deposited golden anchor sites, as well as the finally applied anti-adhesion coating, had the function to level out height differences. The GLAD masks allowed the transfer of the pattern into the wafer by RIE. PMMA did not withstand the etch process very well. It was worn-out three times faster than silicon dioxide. The etch rates of the wafer on the bottom of the holes and through the masks were significantly lower than the ones on the plane surfaces, because the exchange of gases and etch products was hindered.

Two different RIE protocols were developed. CHF_3 in the presence of O_2 promised to etch with a high anisotropy vertical walls. This process is characterized by interchanging periods of the milling of the wafer and the deposition of passivating fluoro-carbons. It was not possible to directly scale down the well established process of etching µm structures vertically with a roughness of the walls in the low nm range to the 10 nm structures obtained by EUV-IL and subsequent GLAD. The achieved anisotropy was low. The plasma was driven at 100 mTorr pressure and supplied with 100 W forward power. The etch rate was measured as 7 (± 2) nm/s inside the holes. A disadvantage of this RIE protocol was the deposition of fluoro-carbons in a ring shaped area around the etched deepenings (see figure 3.5). The deposits remained after lifting-off of the GLAD mask und could only be removed by

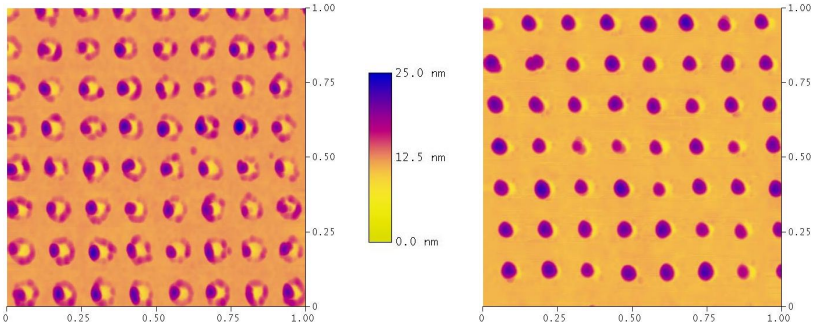

(a) encircling deposits (b) after plasma cleaning

Figure 3.5: **Fluoro-Carbons Remains after RIE.** The AFM images exemplify the problem of the fluoro-carbon remains that were deposited during the RIE with CHF_3 and O_2. The remains occurred around the milled deepenings in which the golden capture sites were located (see 3.5a). The deposits could completely be removed by an oxygen plasma cleaning step (see 3.5b).

an oxygen plasma treatment.

An alternative protocol using SF_6 was developed that etched more isotropically and in a steady mode, not leaving remains. The best performance could be obtained when 40 sccm SF_6 at 80 mTorr were applied to form the plasma, run by 80 W forward power. An etch rate of 10 (± 2) nm/s through the mask was detected.

Using an oxygen plasma flush before starting RIE was a mixed blessing. The plasma effectively removed organic contaminants, such as residues of the development, from the surface of the wafer. The plasma thereby enabled a more homogenously spread beginning of the etch process all over the exposed surface. It, however, proved harmful for the later lift-off. The oxygen radicals transformed the exposed PMMA into a material that was almost inert against organic solvents.

3.4 Lift-off

3.4.1 Removal of Resist

AFM examinations, especially the roughness measurements presented in figure 3.6, showed that spinned photoresist could not be completely removed by the sonication of the sample in acetone (performed in absence of a GLAD mask). Neither the application of an IPA bath after three fresh acetone bathes, nor extensive rinsing of the sample with water solved the problem. However, halogenated organic solvents significantly improved the roughness after lift-off. Dichloromethane generated the best results, chlorobenzene worked comparably well. Solved PMMA was not apt to form aggregates in these chlorinated solvents. In the case of dichloromethane no remaining resist could be found on the surface. Also extensive oxygen plasma treatment led to a similarly clean result.

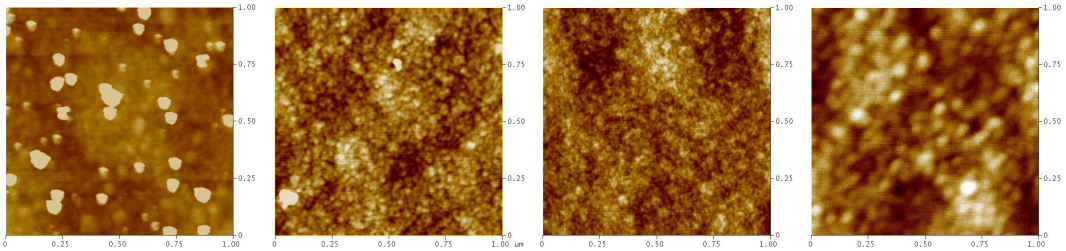

(a) $(CH_3)_2CO$ rms: 1.15 nm (b) C_6H_5Cl rms: 0.44 nm (c) CH_2Cl_2 rms: 0.31 nm (d) O_2 plasma rms: 0.26 nm

Figure 3.6: **PMMA Remainders after different Cleaning Protocols.** The 1 µm AFM scans illustrate the different efficiencies of organic solvents in removing a PMMA layer from a wafer. The comparison of the root mean square values (rms) for the different images clarifed that only the halogenated chemical dichloromethane (see 3.6c) and oxygen plasma (see 3.6d) cleaned the samples entirely. Chlorobenzene (see 3.6b) and even more distinct acetone (see 3.6a) were not able to solubilize all PMMA completely.

3.4.2 Lifting GLAD Mask

After having evaporated the golden anchor sites through the GLAD mask, the metal and the underneath resist had to be removed. Due to the bad wetting of the PMMA by solvents through the small windows in the mask, the GLAD deposited metal could usually not be lifted by the sonication of the samples in organic solvents only. The solvents accessibility to the PMMA had to be improved by etching the metallic mask. Chromium etchant was selective enough not to impact the gold, but it dissolved the PMMA. When chromium and PMMA were removed completely the gold clusters, formed on the mask by the vapor deposition, tended to collapse onto the wafer and often adhered irreversibly to the silicon dioxide. The same situation occurred when a silver layer was used to cap the chromium as a second GLAD mask metal. Up to a thickness of 20 nm these silver coatings did otherwise not show negative effects on the chromium etch supported lift-off.

The chromium etch step was technically demanding. The process had to be observed very well in order to recognize the moment when, after approximately 30 s, the chromium was removed totally. This was indicated by a color change of the surface of the sample. The flipping of the sample while stirring it in the etchant was useful to get rid of the gold clusters on the mask. The multi layer GLAD chromium-silver-chromium did not simplify the lift-off process (see also figure 3.4b). The gold clusters could not be removed effectively enough in a first phase, while the etchant dissolved the top chromium layer.

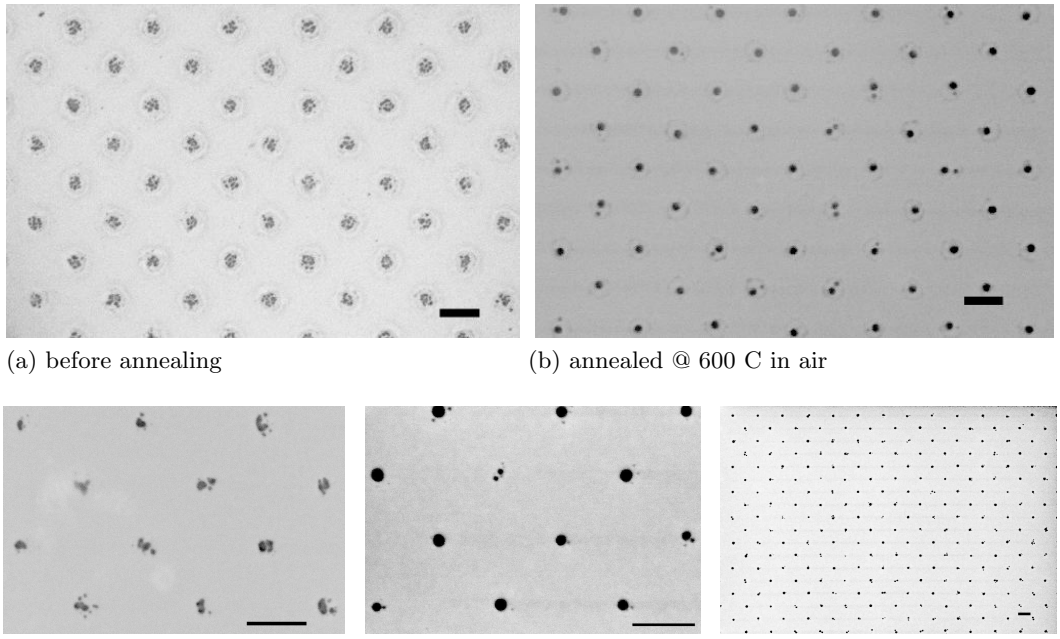

(a) before annealing (b) annealed @ 600 C in air

(c) before annealing (d) annealed @ 510 C in vacuum (e) annealed @ 510 C in vacuum

Figure 3.7: **Annealing Gold Islands.** The evaporated gold islands could be constricted in size and reshaped by thermal annealing. The images 3.7a and 3.7c show two samples after the lift-off of the GLAD mask and directly before the thermal annealing. The images 3.7b and 3.7d/3.7e, respectively, illustrate the appearance of the same samples after the annealing. Both samples were not treated by RIE antecedently to the gold deposition. The achieved dimensions of the anchor sites were 12 (± 3) nm. (scale bars: 100 nm)

3.5 Thermal Annealing

The gold islands, evaporated trough the GLAD mask, were frayed out at their edges. The fringes could be removed and the whole island reshaped towards a spherical contour by thermal annealing (see figure 3.7). Annealing became an important tool for the fabrication of capture protein anchoring sites which were sized in the order of a single DARPin. This process allowed to shrink the diameter of the gold dots by factor of two or better. Only the material located in small spots in the periphery of the islands could not be contracted. On the same time the height of the dots increased by a factor of three. In air, the temperature had to be set below 800 C, in order to avoid the spilling of gold all over the surface. The higher the temperature the better was the constriction and shaping. In accordance with experiments described in literature [59], the volume of the gold dots decreased significantly when heated above 600 C. The duration of the annealing played a minor role.

Gold evaporated on the wafer tended to form clusters. There was a high surface stress due to incompatibilities in the lattice constants at the interface with the silicon dioxide. The wafer had to be coated with at least 5 nm of gold to ensure the formation of a completed layer. The clusters did not adhere strongly to the surface.

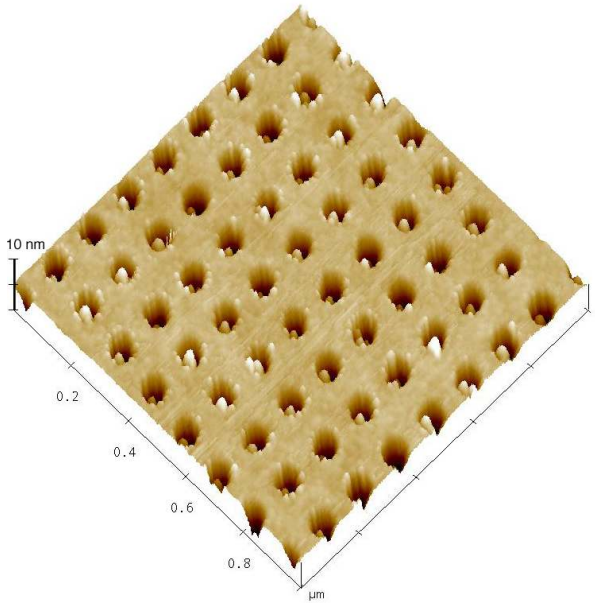

Figure 3.8: **Plunged Capture Sites.** The three-dimensional representation of an AFM scan illustrates an array of gold dots, positioned inside deepenings, milled by RIE. The golden anchor sites are arranged in a centered rectangular lattice with a 141 nm pitch.

It was possible to remove individuals by excessive sonication. The clusters stuck better when they were placed in a depression fabricated by RIE. Chromium adhesion layers mediating between the lattice constants of gold and silicon dioxide irreversibly bound the gold clusters as well. The adhesion layer withstood the lift-off process governed by chromium etch, but reduced the effect of the annealing step drastically.

When evaporating gold through the GLAD mask into the depressions milled by RIE, the dots formation typically started on the walls of the deepenings. The dots had a more distinct roundish appearance compared to the ones evaporated onto the surface of the flat wafer. Correspondingly, the effect of the annealing was less apparent, although the final results (see also figure 3.8) turned out to be comparably well.

3.6 Surface Passivation

3.6.1 Silicon Dioxide Facing

In all performed experiments, PLL-PEG attached selectively to the silicon dioxide. Gold coated surfaces stayed unmodified: AFM scans before and after the application of the PEG derivative showed no differences. The scratching of the AFM tip on the gold surface indicated the adsorption of no molecules as well. The ap-

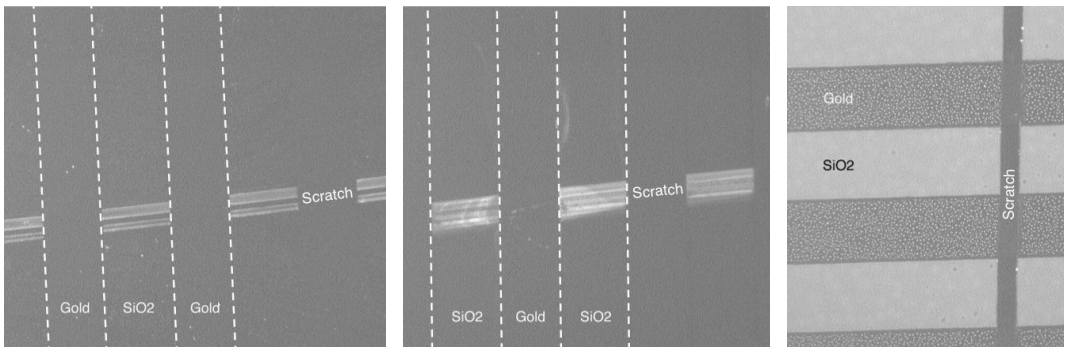

(a) PLL-PEG (b) Star PEG (c) Control

Figure 3.9: **Anti-Adhesive Effect of different PEGylations.** The adsorption of fluorescence labeled Avidin shows the usefulness of the antecedently deposited PEG brushes. On the 90 µm gold striped and PEGylated samples, the fluorescent protein can virtually exclusive be detected where a scratch removed the hydrophilic brushes before absorbing proteins (see 3.9a and 3.9b). The gold quenches the fluorescence completely, as the control (figure 3.9a, no PEG) illustrates best. The horizontal scratch thereon was made after the adsorption of the avidin and removed the fluorescent molecules. The glow of the background of the PLL-PEG layer (see 3.9a) is lower, than the one of Star PEG (see 3.9b).

plication of PLL-PEG was straight forward. The disposal of fluoresce labeled avidin proved the efficiency of the PLL-PEG coating as a passivation agent (see figure 3.9c). AFM scans in liquid showed a high density of coverage of the PLL-PEG coating with brushes. The roughness characteristics of the coating were the same as the ones of the underneath silicon oxide surface. The PEG brushes collapsed when scanned by the AFM tip.

The roughness of the blow dried Star PEG coating was even better than the roughness of the surface of the sample. The anti-adhesive qualities were slightly poorer compared to PLL-PEG (see also figure 3.9c). The same was true for the ability to select between the chemical contrast silicon dioxide-gold. The thickness of the Star PEG coating could be tuned in the range of 3 – 25 nm by setting the spin speed between 1000 and 6000 rpm (see table 3.1). Problems with uncompleted coverage of the samples surface occurred, when the span of time between the activation of the Hydro Stellan molecules by adding water and the appliance onto the sample was to short. The required span of time depended strongly on the concentration of the star shaped molecules in solution. Due to the suboptimal repository that the molecules were delivered in, the concentration was difficult to control. However, concentration varieties had no significant influence on the achieved layer thicknesses.

Table 3.1: **Star PEG Layer Thicknesses.** The size of the Hydro Stellan spin coating can be set by tunig the spin speeds.

spin speed [rpm]	6000	4000	2500	1500	1000
layer thickness [nm]	2 (± 1)	3 (± 1)	5 (± 1)	12 (± 2)	25 (± 4)

3.6.2 Gold Facing

The coating of the gold dots with short hydrophilic thiols should inhibit an irreversible collapse of proteins onto the surface by binding their hydrophobic cores. The coating could as well be useful to limit the number of DARPins bound per dot and was tested on gold striped samples as well as on atomically flat gold, and on unstructured wafer pieces and was studied by AFM in all cases.

MES was the most promising of all tested thiols. It showed a high specificity for the gold surfaces. No MES was found on the silicon dioxide areas of the striped test samples. In combination with PLL-PEG, the PEG brushes showed their habitual anti-adhesive capacity. On the gold, MES formed monolayer like films. On the ultra large atomically flat samples no additional roughness could be found when comparing coated and untreated ones. MPG coated the gold but also formed more than 10 nm thick layers on the silicon dioxide when the sample was not flushed by oxygen plasma antecedently. The plasma increased the specificity almost to the optimum. PLL-PEG was compatible with MPG, it could probably even displace thiols attached to the silicon dioxide. However, a Star PEG coating, selective to the chemical contrast MPG/gold-silicon dioxide, could not be applied anymore. The Hydro Stellan molecules covered the MPG treated gold as well.

The results gained from MUA were not compatible to the ones with MPG and MES. MUA did adhere weakly to the oxide, but could not be removed by PLL-PEG. The roughness of the PEGylated areas increased compared to a thiol free situation. PLL-PEG lost its selectivity: Clusters were formed on the MUA coated gold. A Star PEG layer formation after MUA application was not feasible at all. A rough compound mantled the whole sample after Hydro Stellan disposal.

The fundamentally better compatibility of PLL-PEG with the thiols, together with a superior handling and anti-adhesive nature make this PEG derivative a first choice, when compared to Star PEG. An additional hassle occurred when Star PEG was applied to recessed gold dot arrays. The coating tended to cap the deepenings of the 141 nm pitch nano-patterning and appeared rough, also in between the holes.

3.7 DARPin Fixation

Selective DARPin fixation on gold dots could not be proven. The proteins denatured and collapsed when blow dried. AFM comparison measurements before and after protein application were not meaningful enough, since it was not possible to scan exactly the same range twice. Because of the quenching effect of the gold dots, fluorescence tags were no help either.

When adding DARPins to thiol treated flat test samples, no differences between the adsorption specificities in between MPG and MES could be detected. Additionally applied BMBP inclined to cover the whole surface of the sample, unless applying a harsh washing step after adsorption. The binding of DARPins and BMBPs could not be detected by AFM in air.

Unlike Star PEG, PLL-PEG deposited silicon dioxide surface areas in between the dot patterns were free of macromolecules after applying subsequently DARPins, BMBP, and Avidin.

Chapter 4

Discussion & Conclusions

A path to the manufacturing of nano-structured substrates for a future single cell proteomics chip was successfully developed during this thesis work. All steps of the production process are compatible to mass fabrication. Figure 4.1 gives a schematic overview of the complete manufacturing procedure. Anchor sites of dimensions close to the size of the capture proteins were as well presented, as solutions for the improvement of the absolute resolution of EUV-IL patterning, as the passivation of the surface of a future proteomics chip against non-specific adherence of macromolecules, and as the leveling of the heights of the face of the wafer and the unoccupied binder molecules. All these processes were not depending on the choice of gold as mediator of the binding between the substrate and the DARPins.

4.1 Anchor Sites

4.1.1 Dimensions

For the fabrication of the substrates, EUV-IL patterned PMMA was a suitable starting situation. The improvement of their absolute resolution by GLAD was feasible. Using chromium as deposited material proved to be favorable for the constriction. The smallest holes of an array with a 141 nm pitch was EUV-IL patterned with 120 mJ/cm^2 in a 40 nm thick PMMA layer and could best be narrowed by using an oblique angle of 60°. The optimal chromium deposition rate was 1 nm/s. The evaporation had to be stopped after 90 nm to ensure the homogeneity of the dimensions of the openings. For the final constriction of the holes close to the dimensions of a capture proteins, a double-layered GLAD of silver upon chromium should preferably be chosen. In addition to the constriction effect, the silver smoothened the chromium masks. The cross sections of the openings altered towards a more circle like shape.

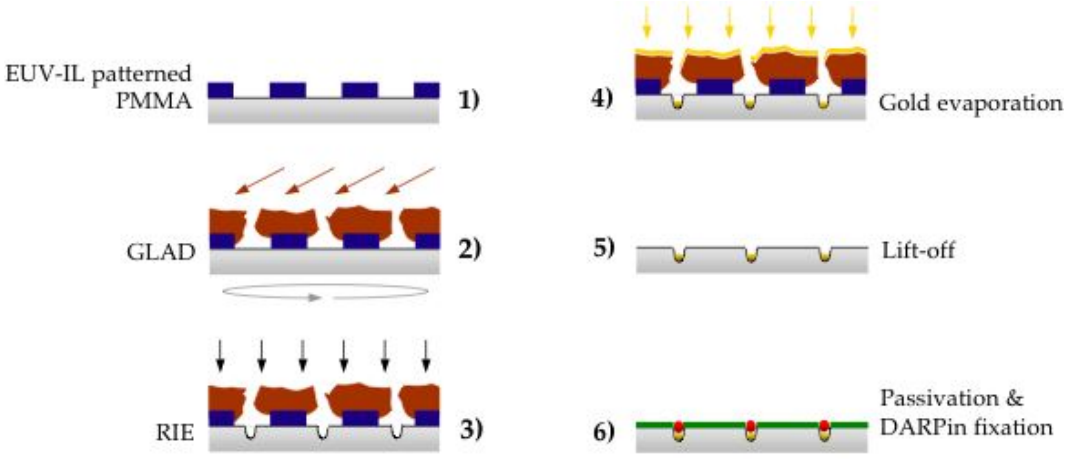

Figure 4.1: **Entire Fabrication Process.** Beginning with EUV-IL patterned PMMA (1), the openings of the wells were constricted by GLAD (2). The Pattern was then transfered into to wafer using RIE through the obliquely deposited GLAD mask (3). The evaporation of the gold was responsible for the production of the anchor sites (4). After lift-off (5) and annealing, the substrate was ready for the applications of the anti-adhesive coatings and the anchoring of the cognitive molecules (6).

More than 20 nm of silver must not be deposited at an oblique angle of 25°, using a deposition rate of 4 nm/s. Thicker silver layers would inhibit a successful lift-off.

Since it was not realistic to implement a cooling system for the rotating sample, the thermal evaporation was time-critical. The deposition rates had to be optimized between the conflicting areas of mask graininess and facilitation of the lift-off. For the oblique angles, the optimum between the degree of constriction of the holes and the enabling of the lift-off had to be found as well.

For the setting of the height level between the top of the golden capture sites and the surroundings, RIE emerged as a strong tool. Two different equally suitable protocols were developed for the etching trough the GLAD masks, antecedent to the evaporation of gold. The minimal amount of deposited gold, 5 nm thick islands, could successfully be contracted by an annealing step. The procedure appeared to be more effective in vacuum, as well as working with temperatures close to the maximum of 800 C.

4.1.2 Uniformity

It might be worthwhile to expose a sample by EUV-IL with less than 120 mJ/cm ^{2}. It was not evaluated, if this value would be the true minimal clearance dose of the arrays with a 141 nm pitch. Open holes, exposed with a lower dose promise to be smaller. As long as the homogeneity over the whole array is given, and a RIE step is executed before depositing the gold islands, the perfect clearance of windows in the PMMA would not necessarily be required. Never the less, the heterogeneity of

the hole size increases drastically at underexposed samples.

In order to achieve gold dots with hight varieties better than 0.5 nm, a variety of the dimension of the hole size better than ±10 % was required. Due to the clustering of the gold and the annealing effect, the amount of deposited metal was crucial for the obtained heights of the capture sites. Differences in the etch depth were small in comparison and the discrepancies of the mean values systematically had a balancing impact on the total error of the leveling.

The lattices of the gold islands could be produced sufficiently large for future proteomics chip applications and were virtually free of defects. The anchor sites had dimensions of 10 – 15 nm. An interspace between two fields of the same size as the fields is realistic for the envisaged application. This work has not identified any obstacles, militating the outlined capacity of a future chip. Contrariwise, the feasibility of our vision about the geometries of the substrates was largely proven.

4.2 Passivation and Protein Anchoring

Two different anti-adhesion coatings, PLL-PEG and Star PEG were evaluated. Only PLL-PEG assures that the nm sized, plunged capture sites were not covered by the anti-adhesive coating. Layers of Star PEG do have a comparably well effect of passivation, but are less selective and do show less compatibility with all other studied surface modifications. The advantage of Star PEG, its possibility to tune the thickness of the coating and to correct height differences in order to level inequalities between the capture sites and surrounding, is partly relativized by the difficult applicability and the strength of RIE to level out inequalities in the heights of the gold islands and the wafer.

Problems due to the roughness of the surface should not occur when continuing with this chip project. The PEGylated surfaces are not rougher than the polished wafers with thermal oxide coating, although the PEG brushes collapse when scanned by the AFM tip.

The complexity when adsorbing a series of cognitive proteins, that have to bind each other, increases disproportionately high per any additionally applied macromolecule. The analysis of potential failures is demanding, as well as the arrangement of adequate negative controls. The adsorption process of the proteins must be observed successively. The first step, the visualization of the anchored DARPins should be simplified by the fusion of large reporters.

Chapter 5

Outlook

The proof of the possibility to anchor single or only a few functional proteins on the gold islands should be the next experimental step towards a single cell proteomics chip. The verification should be done by AFM in liquid, since the native proteins can only be studied in buffer solution. A well defined area of the array of anchor sites has to be scanned before and after applying the capture proteins, to demonstrate the successful anchoring. The recovery of an already scanned region is an experimental difficulty. The most straight forward experimental setup would include the implementation of the fixation of the proteins to the anchor sites inside the liquid cell of the AFM itself.

The optical detection of the patterning is challenging. An AFM optimized for biological samples has to be combined with a high quality optical microscope. To the authors knowledge all available apparatus in this setup have an illumination from the backside, wherefore transparent probes are required. This imposes a replacement of the silicon by glass wafers. The glass can be treated the same as the silicon dioxide. In particular will the insulating characteristics further on enable fluorescence experiments. The RIE rates might differ marginally.

Should the size of the anchor sites obtainable with the manufacturing protocol described in this work turn out to be too large for single or just a few capture proteins, the deposition of single gold nanospheres in pre hole-patterned substrates should be tried. Two different methods are available. Block copolymer micelle lithography [75] makes use of the possibility to remove organic material which envelopes gold particles by plasma treatment. Single nm sized gold particles can be enlarged by coating to the dimension of holes in pre-structured photoresist, up to 100 nm. This micelles can be spinned on the patterned sample till they form a monolayer. Those sitting on the resist can selectively be removed by lifting the resist. In a different approach the only slightly enlarged gold colloids are dip-coated into

pre-patterned deepenings out of a suspension, making use of capillary forces [76]. Large, defect-free arrays are a big challenge with both methods. Missing colloids are just as difficult to avoid, as the existence wrong placed of extra particles.

If the anchoring of the capture proteins on the gold islands by the cysteine tag should fail, as alternative way the binding via oligohistidines could be chosen. Multivalent chelator heads containing three nitrilotriacetic acid moieties do bind hexahistidine tags with a sufficient affinity [77] were shown to successfully attach to gold colloids.

Appendix A

Acknowledgements

First of all, I thank Prof. Dr. Andreas Engel and Prof. Dr. Jens Gobrecht for giving me the opportunity to work on this highly interesting and challenging project.

Above all, I would like to express my gratitude to Dr. Celestino Padeste for his great support and encouragement during the whole thesis work.

I would like to acknowledge all members of the Laboratory for Micro- and Nanotechnology at the Paul Scherrer Institut, especially Dr. Harun Solak for providing EUV-IL structures and access to the beamline, Patrick Farquet for the help with the liquid cell of the AFM, Christian Daiss for his help at the beamline, Dr. Christian David and Dr. Yasim Ekinci for their help with the evaporation system, Dr. Harald Sehr and Sandro Bellini for introducing me to dry etching, Dr. Vaida Auzelyte for her help, while testing new development protocols and Roger Bischofberger (Applied microSWISS) for providing chromium etch agent.

Furthermore, I would like to acknowledge Prof. Dr. Andreas Plückthun and Dr. Hans Kaspar Binz from the Department of Biochemistry of the University of Zürich for providing proteins.

At the Institute of Physics of the University of Basel, I would also like to thank PD Dr. Martin Hegner for his hints and chemicals and Prof. Dr. Christian Schönenberger for the opportunity to use his facilities.

Many thanks also to Prof. Dr. Wolfgang Meier and all the others who helped me along with valuable discussions.

Appendix B

Bibliography

(1) S. Hanash, *Disease proteomics.*, Nature **422**, 226 (2003).

(2) S. Souchelnytskyi, *Bridging proteomics and systems biology: what are the roads to be traveled?*, Proteomics **5**, 4123 (2005).

(3) S. Fields, *Proteomics in genomeland.*, Science **291**, 1221 (2001).

(4) S. P. Gygi, Y. Rochon, B. R. Franza, and R. Aebersold, *Correlation between protein and mRNA abundance in yeast.*, Mol Cell Biol **19**, 1720 (1999).

(5) P. Cutler, *Protein arrays: the current state-of-the-art.*, Proteomics **3**, 3 (2003).

(6) G. C. Adam, E. J. Sorensen, and B. F. Cravatt, *Proteomic profiling of mechanistically distinct enzyme classes using a common chemotype.*, Nat Biotechnol **20**, 805 (2002).

(7) Y. Lill, M. A. Lill, B. Fahrenkrog, K. Schwarz-Herion, S. Paulillo, U. Aebi, and B. Hecht, *Single hepatitis-B virus core capsid binding to individual nuclear pore complexes in Hela cells.*, Biophys J **91**, 3123 (2006).

(8) H. P. Lang, M. Hegner, and C. Gerber, *Cantilever array sensors.*, Mat Today **8**, 30 (2005).

(9) N. Backmann, C. Zahnd, F. Huber, A. Bietsch, A. Plückthun, H.-P. Lang, H.-J. Güntherodt, M. Hegner, and C. Gerber, *A label-free immunosensor array using single-chain antibody fragments.*, Proc Natl Acad Sci U S A **102**, 14587 (2005).

(10) M. Pawlak, E. Schick, M. A. Bopp, M. J. Schneider, P. Oroszlan, and M. Ehrat, *Zeptosens' protein microarrays: a novel high performance microarray platform for low abundance protein analysis.*, Proteomics **2**, 383 (2002).

(11) V. W. Jones, J. R. Kenseth, M. D. Porter, C. L. Mosher, and E. Henderson, *Microminiaturized immunoassays using atomic force microscopy and compositionally patterned antigen arrays.*, Anal Chem **70**, 1233 (1998).

(12) H. Zhu and M. Snyder, *Protein chip technology.*, Curr Opin Chem Biol **7**, 55 (2003).

(13) M. F. Templin, D. Stoll, M. Schrenk, P. C. Traub, C. F. Vöhringer, and T. O. Joos, *Protein microarray technology.*, Trends Biotechnol **20**, 160 (2002).

(14) A. Plückthun, P. Vettiger, U. Staufer, and A. Engel, Single cell proteomics., Poster, 2006.

(15) S. C. Minne, J. D. Adams, G. Yaralioglu, S. R. Manalis, A. Atalar, and C. F. Quate, *Centimeter scale atomic force microscope imaging and lithography.*, Appl Phys Lett **73**, 1742 (1998).

(16) P. Vettiger, M. Despont, U. Drechsler, U. Dürig, W. Häberle, M. I. Lutwyche, H. E. Rothuizen, R. Stutz, R. Widmer, and G. K. Binnig, *The "Millipede" – more than one thousand tips for future AFM data storage.*, IBM J Res Dev **44**, 323 (2000).

(17) P. Vettiger, G. Cross, M. Despont, U. Drechsler, U. Dürig, B. Gotsmann, W. Häberle, M. A. Lantz, H. E. Rothuizen, R. Stutz, and G. K. Binnig, *The "Millipede" – nanotechnology entering data storage.*, IEEE Trans Nanotechnol **1**, 39 (2002).

(18) L. Aeschimann, A. Meister, T. Akiyama, Benjamin, W. Chui, P. Niedermann, H. Heinzelmann, N. F. D. Rooij, U. Staufer, and P. Vettiger, *Scanning probe arrays for life sciences and nanobiology.*, Microelectron Eng **83**, 1698 (2006).

(19) H. K. Binz, M. T. Stumpp, P. Forrer, P. Amstutz, and A. Plückthun, *Designing repeat proteins: well-expressed, soluble and stable proteins from combinatorial libraries of consensus ankyrin repeat proteins.*, J Mol Biol **332**, 489 (2003).

(20) P. Forrer, M. T. Stumpp, H. K. Binz, and A. Plückthun, *A novel strategy to design binding molecules harnessing the modular nature of repeat proteins.*, FEBS Lett **539**, 2 (2003).

(21) A. Kohl, H. K. Binz, P. Forrer, M. T. Stumpp, A. Plückthun, and M. G. Grütter, *Designed to be stable: crystal structure of a consensus ankyrin repeat protein.*, Proc Natl Acad Sci U S A **100**, 1700 (2003).

(22) H. K. Binz, P. Amstutz, A. Kohl, M. T. Stumpp, C. Briand, P. Forrer, M. G. Grütter, and A. Plückthun, *High-affinity binders selected from designed ankyrin repeat protein libraries.*, Nat Biotechnol **22**, 575 (2004).

(23) H. K. Binz and A. Plückthun, *Engineered proteins as specific binding reagents.*, Curr Opin Biotechnol **16**, 459 (2005).

(24) C. Zahnd, P. Amstutz, and A. Plückthun, *Ribosome display: selecting and evolving proteins in vitro that specifically bind to a target.*, Nat Methods **4**, 269 (2007).

(25) S. Kossek, C. Padeste, L. X. Tiefenauer, and H. Siegenthaler, *Localization of individual biomolecules on sensor surfaces*, Biosens Bioelectron **13**, 31 (1998).

(26) P. Kingshott and H. J. Griesser, *Surfaces that resist bioadhesion.*, Curr Opin Solid State Mater Sci **4**, 403 (1999).

(27) S. Pasche, M. Textor, L. Meagher, N. D. Spencer, and H. J. Griesser, *Relationship between interfacial forces measured by colloid-probe atomic force microscopy and protein resistance of poly (ethylene glycol)-grafted poly (L-lysine) adlayers on niobia surfaces.*, Langmuir **21**, 6508 (2005).

(28) T. Drobek, N. D. Spencer, and M. Heuberger, *Compressing PEG brushes.*, Macromolecules **38**, 5254 (2005).

(29) M. Heuberger, T. Drobek, and N. D. Spencer, *Interaction forces and morphology of a protein-resistant poly (ethylene glycol) layer.*, Biophys J **88**, 495 (2005).

(30) R. Kjellander and E. Florin, *Water structure and changes in thermal stability of the system poly (ethylene oxide)-water.*, J Chem Soc, Faraday Trans **1**, 2053 (1981).

(31) M. Heuberger, T. Drobek, and J. Vörös, *About the role of water in surface-grafted poly (ethylene glycol) layers.*, Langmuir **20**, 9445 (2004).

(32) R. Michel, S. Pasche, M. Textor, and D. G. Castner, *Influence of PEG architecture on protein adsorption and conformation.*, Langmuir **21**, 12327 (2005).

(33) W. Hu, K. Sarveswaran, M. Lieberman, and G. H. Bernstein, *Sub-10 nm electron beam lithography using cold development of poly (methylmethacrylate).*, J Vac Sci Technol B **22**, 1711 (2004).

(34) Piner, Zhu, Xu, Hong, and Mirkin, *"Dip-Pen" nanolithography*, Science **283**, 661 (1999).

(35) G.-Y. Liu and N. A. Amro, *Positioning protein molecules on surfaces: a nanoengineering approach to supramolecular chemistry.*, Proc Natl Acad Sci U S A **99**, 5165 (2002).

(36) S. Xu and G.-Y. Liu, *Nanometer-scale fabrication by simultaneous nanoshaving and molecular self-assembly.*, Langmuir **13**, 127 (1997).

(37) K. Wadu-Mesthrige, N. A. Amro, J. C. Garno, S. Xu, and G. Liu, *Fabrication of nanometer-sized protein patterns using atomic force microscopy and selective immobilization.*, Biophys J **80**, 1891 (2001).

(38) H. Agheli, J. Malmström, E. M. Larsson, M. Textor, and D. S. Sutherland, *Large area protein nanopatterning for biological applications.*, Nano Lett **6**, 1165 (2006).

(39) P. Hanarp, D. S. Sutherland, J. Gold, and B. Kasemo, *Control of nanoparticle film structure for colloidal lithography*, Colloids Surf A **214**, 23 (2003).

(40) P. Hanarp, M. Käll, and D. S. Sutherland, *Optical properties of short range ordered arrays of nanometer gold disks prepared by colloidal lithography.*, J Phys Chem B **107**, 5768 (2003).

(41) H. W. Deckman and J. H. Dunsmuir, *Natural lithography*, Appl Phys Lett **41**, 377 (1982).

(42) J. C. Hulteen and R. P. V. Duyne, *Nanosphere lithography: A materials general fabrication process for periodic particle array surfaces*, J Vac Sci Technol A **13**, 1553 (1995).

(43) C. L. Haynes and R. P. V. Duyne, *Nanosphere lithography: a versatile nanofabrication tool for studies of size-dependent nanoparticle optics.*, J Phys Chem B **105**, 5599 (2001).

(44) A. Kumar and G. M. Whitesides, *Features of gold having micrometer to centimeter dimensions can be formed through a combination of stamping with an elastomeric stamp and an alkanethiol "ink" followed by chemical etching.*, Appl Phys Lett **63**, 2002 (1993).

(45) A. P. Quist, E. Pavlovic, and S. Oscarsson, *Recent advances in microcontact printing.*, Anal Bioanal Chem **381**, 591 (2005).

(46) H. H. Solak, D. He, S. S.-G. W. Li, F. Cerrina, B. H. Sohn, X. M. Yang, and P. Nealey, *Exposure of 38 nm period grating patterns with extreme ultraviolet interferometric lithography.*, Appl Phys Lett **75**, 2328 (1999).

(47) H. Solak, C. David, J. Gobrecht, L. Wang, and F. Cerrina, *Multiple-beam interference lithography with electron beam written gratings.*, J Vac Sci Technol B **20**, 2844 (2002).

(48) H. Solak, C. David, J. Gobrecht, V. Golovkina, F. Cerrina, S. Kim, and P. Nealey, *Sub-50 nm period patterns with EUV interference lithography.*, Microelectron Eng **67/68**, 56 (2003).

(49) A. Küller, W. Eck, V. Stadler, W. Geyer, and A. Gölzhäuser, *Nanostructuring of silicon by electron-beam lithography of self-assembled hydroxybiphenyl monolayers.*, Appl Phys Lett **82**, 3776 (2003).

(50) A. Gölzhäuser, W. Eck, W. Geyer, V. Stadler, T. Weimann, P. Hinze, and M. Grunze, *Chemical nanolithography with electron beams.*, Adv Mater **13**, 806 (2001).

(51) U. Schmelmer, R. Jordan, W. Geyer, W. Eck, A. Gölzhäuser, M. Grunze, and A. Ulman, *Surface-initiated polymerization on self-assembled monolayers: amplification of patterns on the micrometer and nanometer scale.*, Angew Chem Int Ed Engl **42**, 559 (2003).

(52) Q. He, Y. Tian, A. Küller, M. Grunze, A. Gölzhäuser, and J. Li, *Self-assembled molecular pattern by chemical lithography and interfacial chemical reactions.*, J Nanosci Nanotechnol **6**, 1838 (2006).

(53) A. Biebricher, A. Paul, P. Tinnefeld, A. Gölzhäuser, and M. Sauer, *Controlled three-dimensional immobilization of biomolecules on chemically patterned surfaces.*, J Biotechnol **112**, 97 (2004).

(54) H. Namatsu, Y. Takahashi, K. Yamazaki, T. Yamaguchi, M. Nagase, and K. Kurihara, *Three-dimensional siloxane resist for the formation of nanopatterns with minimum linewidth fluctuations.*, J Vac Sci Technol B **16**, 69 (1998).

(55) H. Namatsu, T. Yamaguchi, M. Nagase, K. Yamazaki, and K. Kurihara, *Nanopatterning of a hydrogen silsesquioxane resist with reduced linewidth fluctuations.*, Microelectron Eng **41/42**, 331 (1998).

(56) F. C. M. J. M. van Delft, J. P. Weterings, A. K. van Langen-Suurling, and H. Romijn, *Hydrogen silsesquioxane/novolak bilayer resist for high aspect ratio nanoscale electron-beam lithography.*, J Vac Sci Technol B **18**, 3419 (2000).

(57) K. Robbie, M. J. Brett, and A. Lakhtakia, *First thin film realization of a helicoidal bianisotropic medium.*, J Vac Sci Technol A **13**, 2991 (1995).

(58) K. Robbie and M. J. Brett, *Sculptured thin films and glancing angle deposition: growth mechanics and applications.*, J Vac Sci Technol A **15**, 1460 (1997).

(59) B. J. Y. Tan, C. H. Sow, T. S. Koh, K. C. Chin, A. T. S. Wee, and C. K. Ong, *Fabrication of size-tunable gold nanoparticles array with nanosphere lithography, reactive ion etching, and thermal annealing.*, J Phys Chem B **109**, 11100 (2005).

(60) P. Morf, *Self-assembled monolaysers beyond thiols: Dithiocabamates - from pure layers to ternary assembly systems*, PhD thesis, University of Basel, 2005.

(61) N.-P. Huang, R. Michel, J. Vörös, M. Textor, R. Hofer, A. Rossi, D. L. Elbert, J. A. Hubbell, and N. D. Spencer, *Poly (L-lysine)-g-poly (ethylene glycol) layers on metal oxide surfaces: surface-analytical characterization and resistance to serum and fibrinogen adsorption.*, Langmuir **17**, 489 (2001).

(62) G. L. Kenausis, J. Vörös, D. L. Elbert, N. Huang, R. Hofer, L. Ruiz-Taylor, M. Textor, J. A. Hubbell, and N. D. Spencer, *Poly (L-lysine)-g-poly (ethylene glycol) layers on metal oxide surfaces: attachment mechanism and effects of polymer architecture on resistance to protein adsorption.*, J Phys Chem B **104**, 3298 (2000).

(63) W. Franks, S. Tosatti, F. Heer, P. Seif, M. Textor, and A. Hierlemann, *Patterned cell adhesion by self-assembled structures for use with a CMOS cell-based biosensor.*, Biosens Bioelectron **22**, 1426 (2007).

(64) E. V. Amirgoulova, J. Groll, C. D. Heyes, T. Ameringer, C. Röcker, M. Möller, and G. U. Nienhaus, *Biofunctionalized polymer surfaces exhibiting minimal interaction towards immobilized proteins.*, Chemphyschem **5**, 552 (2004).

(65) J. Groll, J. Fiedler, E. Engelhard, T. Ameringer, S. Tugulu, H.-A. Klok, R. E. Brenner, and M. Moeller, *A novel star PEG-derived surface coating for specific cell adhesion.*, J Biomed Mater Res A **74**, 607 (2005).

(66) J. Groll, K. Albrecht, P. Gasteier, S. Riethmueller, U. Ziener, and M. Moeller, *Nanostructured ordering of fluorescent markers and single proteins on substrates.*, Chembiochem **6**, 1782 (2005).

(67) J. Groll, Z. Ademovic, T. Ameringer, D. Klee, and M. Moeller, *Comparison of coatings from reactive star shaped PEG-stat-PPG prepolymers and grafted linear PEG for biological and medical applications.*, Biomacromolecules **6**, 956 (2005).

(68) M. Hegner, P. Wagner, and G. Semenza, *Ultralarge atomically flat template-stripped Au surfaces for scanning probe microscopy.*, Surf Sci **291**, 39 (1993).

(69) S. Pasche, S. M. D. Paul, J. Vörös, N. D. Spencer, and M. Textor, *Poly(L-lysine)-graft-poly (ethylene glycol) assembled monolayers on niobium oxide surfaces: a quantitative study of the influence of polymer interfacial architecture on resistance to protein adsorption by ToF-SIMS and in situ OWLS.*, Langmuir **19**, 9216 (2003).

(70) S. G. P. Tosatti, *Functionalized titanium surfaces for biomedical applications: physico-chemical characterization and biological in vitro evaluation.*, PhD thesis, Swiss Federal Institut of Technology Zürich, 1999.

(71) W. Hu, K. Sarveswaran, Marya, Lieberman, and G. H. Bernstein, *High-resolution electron beam lithography and DNA nano-patterning for molecular QCA.*, IEEE Trans Nanotechnol **4**, 312 (2005).

(72) L. E. Ocolaa and A. Stein, *Effect of cold development on improvement in electron-beam nanopatterning resolution and line roughness.*, J Vac Sci Technol B **24**, 3061 (2006).

(73) S. Yasin, D. G. Hasko, and H. Ahmed, *Fabrication of $<$5 nm width lines in poly (methyl methacrylate) resist using a water:isopropyl alcohol developer and ultrasonically-assisted development.*, Appl Phys Lett **78**, 2760 (2001).

(74) D. R. Lide, *CRC handbook of chemistry and physics.*, CRC Press, 72 edition, 1991.

(75) R. Glass, M. Möller, and J. P. Spatz, *Block copolymer micelle nanolithography.*, Nanotechnology **14**, 1153 (2003).

(76) F. Juillerat, H. H. Solak, P. Bowen, and H. Hofmann, *Fabrication of large-area ordered arrays of nanoparticles on patterned substrates.*, Nanotechnology **16**, 1311 (2005).

(77) S. Lata, A. Reichel, R. Brock, R. Tampé, and J. Piehler, *High-affinity adaptors for switchable recognition of histidine-tagged proteins.*, J Am Chem Soc **127**, 10205 (2005).

Appendix C

Abbreviations

AFM	Atomic force microscopy
BMBP	Biotinylated maltose binding protein
DARPin	Designed ankyrin repeat protein
EBL	Electron beam lithography
EUV	Extreme ultraviolet
EUV-IL	EUV interference lithography
GLAD	Glancing angle deposition
IPA	Isopropyl alcohol
MES	Sodium 2-mercaptoethane sulfonate
MIBK	Methyl isobutyl ketone
MPG	N-(2-Mercaptopropionyl) glycine
MUA	Mercaptoundecanoic acid
PEG	Poly (ethylene glycole)
PLL	Poly (L)-lysine
PLL-PEG	PLL grafted PEG
PMMA	Poly (methyl methacrylate)
PTFE	Poly (tetrafluoro ethylene)
RIE	Reactive ion etching
rms	Root mean square
SEM	Scanning electron microscopy

List of Figures

List of Tables

Part II

Laboratory Notebook